Animated simulation of light transport in tissues

Lihong V. Wang, Steven L. Jacques

Lihong V. Wang, Steven L. Jacques, "Animated simulation of light transport in tissues," Proc. SPIE 2134, Laser-Tissue Interaction V; and Ultraviolet Radiation Hazards, (17 August 1994); doi: 10.1117/12.182939

SPIE.

Event: OE/LASE '94, 1994, Los Angeles, CA, United States

Animated Simulation of Light Transport in Tissues

Lihong Wang and Steven L. Jacques

Laser Biology Research Laboratory - Box 17
The University of Texas M. D. Anderson Cancer Center
1515 Holcombe Boulevard, Houston, Texas 77030

ABSTRACT

Time-resolved light transport in composite tissues is simulated using the Monte Carlo technique. Snapshots of spatial distributions of physical quantities, including light absorption rate, light fluence rate, and diffuse reflectance rate, are presented. Such multiple snapshots with a given time interval can be shown sequentially to achieve an animation effect. This animated simulation is a tool that aids in the general understanding of light transport in tissues. For example, the simulation of time-resolved spatial distribution of light fluence rate inside a tissue illustrates how fast light is dispersed inside tissues. The simulation of diffuse reflectance rate as a function of time of a short-pulsed laser incident upon a piece of tissue containing a buried object shows that early reflected light does not carry imaging information of the object. The imaging quality of the object can thus be improved by rejecting the early-arriving reflected light.

INTRODUCTION

In laser-tissue interactions, it is important to model light transport in tissues, which are turbid media. Modeling helps understand the mechanism of laser-tissue interactions, provides algorithms for laser diagnosis of diseases, and guides dosimetry for laser therapy of diseases. Among the available models are Monte Carlo simulations,[1–7] diffusion theories,[8–14] finite difference methods,[15] finite element methods,[16] and hybrid models of Monte Carlo-diffusion theory.[17,18]

The general use of Monte Carlo simulations is well established in the literature.[1–7] Our Monte Carlo simulation program for multi-layered tissues has been distributed in the public domain for over a year.[19] The program can be downloaded by anonymous ftp (File Transfer Protocol) to laser.mda.uth.tmc.edu (129.106.60.92). Monte Carlo simulations are the most accurate models but suffer from long computational requirements. Analytically solvable diffusion theories for simple geometries are the fastest but are not flexible enough to solve complex geometries and lack accuracy near the light source and sometimes near the boundaries. Finite difference methods and finite element methods are sometimes used to solve radiative transfer equations with the diffusion approximation. They are flexible and considerably faster than Monte Carlo simulations but are subject to the limitations of the diffusion approximation. The hybrid of Monte Carlo-diffusion theory combines the accuracy advantage of the Monte Carlo simulations with the speed advantage of the diffusion theories.

We have recently implemented a more general machine-portable time-resolved Monte Carlo simulation program in C for tissues with buried objects. The program thus far accepts spheres, rectangular boxes with faces parallel to the Cartesian coordinate axes of the tissue system, and cylinders oriented along one of the three Cartesian coordinate axes.

Both our programs compute light distributions according to tissue geometries and optical properties. The tissue optical properties include refractive index, absorption coefficient, scattering coefficient, and anisotropy factor.

We applied the time-resolved Monte Carlo program to several examples of tissue configurations. The simulation results are presented in selected multiple frames as a function of time

0-8194-1429-8/94/$6.00

to show the time course of 2-D images of the light transport. Running the frames sequentially on a computer generates an animation effect that shows the dynamic light transport in tissues.

METHODS

To compute light distributions according to tissue geometries and optical properties, including refractive index (n), absorption coefficient (μ_a), scattering coefficient (μ_s), and anisotropy factor (g), we have written a Monte Carlo program in C for tissues with buried objects. We use the delta-scattering technique[20] for photon tracing to greatly simplify the algorithm because this technique allows a photon packet to be traced without worrying about the interfaces between tissues. This technique can be used only for refractive-index-matched tissues, although it allows the ambient clear media (e.g., air) and the tissue to have mismatched refractive indices.

We assume the tissue system has multiple tissue types with matched refractive indices. The interaction coefficient of the ith tissue type, defined as the sum of μ_a and μ_s, is denoted by μ_i. The technique is briefly summarized as follows.

1. Define a majorant interaction coefficient μ_m, $\mu_m \geq \mu_i$ for all i.
2. Select a distance R,

$$R = -\ln(\xi) / \mu_m, \tag{1}$$

where ξ is a uniformly distributed random number between 0 and 1 ($0 < \xi \leq 1$). Then, determine the tentative next collision site $\mathbf{r}_k'$ by:

$$\mathbf{r}_k' = \mathbf{r}_{k-1} + R\,\mathbf{u}_{k-1}, \tag{2}$$

where $\mathbf{r}_{k-1}$ is the current site and $\mathbf{u}_{k-1}$ is the direction of the flight.

3. Play a rejection game:
   a. With a probability of $\mu(\mathbf{r}_k')/\mu_m$, accept this point as a real interaction site ($\mathbf{r}_k = \mathbf{r}_k'$);
   b. Otherwise, do not accept $\mathbf{r}_k'$ as a real interaction site but select a new path starting from $\mathbf{r}_k'$ with the unchanged direction $\mathbf{u}_{k-1}$ (i.e., set $\mathbf{r}_{k-1} = \mathbf{r}_k'$ and return to Step 2).

The validity can be easily understood. Let us introduce an imaginary interaction event that changes neither the weight nor the direction of the photon. This definition implies that such imaginary interactions are not physically observable, i.e., they can be introduced with any interaction coefficient at any point. Now if we assume that the majorant interaction coefficient (μ_m) is a sum of the real (μ_{re}) and imaginary (μ_{im}) interaction coefficients, then in the procedure outlined above, a fraction of the interactions,

$$1 - \mu_{re}/\mu_m = \mu_{im}/\mu_m \tag{3}$$

are imaginary interactions. Looking at it from another angle, we see that on the average, for every μ_m total interactions, there will be μ_{re} interactions accepted as real interactions. The mean free path for the majorant interactions in the delta-scattering method is $1/\mu_m$ and the mean free path for the real interactions in the directe method is $1/\mu_{re}$. Therefore, the photon will move to the correct interaction site using the delta-scattering technique as it would using the direct method, i.e.,

$$\mu_m(1/\mu_m) = \mu_{re}\,(1/\mu_{re}), \tag{4}$$

where the left-hand side is the average distance traveled by the photon packet with μ_m total steps or with μ_{re} real interactions in the delta-scattering method and the right-hand side is the average distance traveled with μ_{re} real interactions in the direct method.

During the tracing of each weighted photon, the light absorption, reflectance, or transmittance are correspondingly scored into different arrays according to the spatial and temporal positions of the

photon. Multiple photons (1×10^5-1×10^7) are traced to achieve an acceptable statistical variation. The averaged results at different times are generated.

To use the imaging program with the animation ability from the National Center for Supercomputing Applications (NCSA), we extract multiple frames from the simulation results and save them in the Hierarchical Data Format (HDF). The NCSA imaging program can read the frames and play them back as animation. Interested readers can obtain the animation sequences and the imaging program by contacting the authors.

RESULTS

The difference in fluence rate between an isotropic point source and a pencil beam inside an infinite tissue is demonstrated in Fig. 1. The optical properties of dermis in the 440 nm wavelength are used for the simulations.[21] The light from the isotropic source remains isotropic and moves outward from the source point, whereas the light from the pencil source travels downward while being dispersed by the scattering medium. The sizes of the outer edges in the light distributions originated from the two sources at a given time are about the same, although the light-distribution patterns are quite different in the beginning. After light travels 5 picoseconds (ps), the fluence rate caused by the pencil beam approaches isotropic. Since one transport mean free path (mfp'), defined as $1/[\mu_a + \mu_s (1-g)]$, of the tissue is $1/[1.4 + 350 \times (1-0.8)] = 0.014$ cm, the distance that the light travels in 5 ps, computed as 0.03 (cm/ps) $\times$ 5 (ps) / 1.37 = 0.109 cm, is 7.8 mfp'. In other words, the fluence rate is approximately isotropic after light travels 7.8 mfp'.

The integrated fluence rate at x = 0 as a function of z in Fig. 1p is plotted in Fig. 2. The smoothed curve shows that the integrated fluence rate is approximately symmetrical about the z-position that is 1 mfp' from the source position.

The energy-absorption rates integrated along the y-axis are computed for a pencil beam incident upon a semi-infinite dermis tissue (Figs. 3a-h) and a semi-infinite dermis tissue with buried high-absorbing melanin (Figs. 3i-p). The optical properties of dermis and melanin in the 440 nm wavelength are used for the simulations.[21] In Figs. 3a-h, an energy center traveling downward can be observed in the early stage of the propagation and is dispersed with propagation as a result of the scattering. In Figs. 3i-p, the energy center is not as strong and does not travel as deep as that in Figs. 3a-h as a result of the high absorption of the melanin.

The diffuse reflectance patterns of a circular laser beam incident upon a semi-infinite tissue (Figs. 4a-h) and a semi-infinite tissue with a buried absorber (Figs. 4i-p) are simulated. In Figs. 4a-h, the center of the reflectance pattern stays the brightest and the pattern grows symmetrically with time as a result of scattering. In Figs. 4i-p, the pattern grows as fast as that in Figs. 4a-h, but a dark spot in the center starts to appear as time elapses because of the buried absorber. The round-trip time between the light entry point and the top of the sphere is 2×0.1 (cm) / 0.03 (cm/ps) $\times$ 1.37 = 9.1 ps, but the effect of the absorber only appears after Fig. 4l that has a 52.5-ps delay.

DISCUSSION

Figs. 1, 3, and 4 present only a few selected frames of larger animation sequences in false colors. The goal is to give the reader a feeling of dynamic light propagation in tissues. Figs. 1 and 2 show that when light is delivered into tissues interstitially through a fiber with an isotropic tip or a regular straight tip that is considered small in diameter compared with 1 mfp', the light distribution after light travels a few mfp' caused by the two tips are equivalent except for a spatial shift of 1 mfp'. Of course the difference is greater when the fiber tip is large compared with 1 mfp' of the tissue. Fig. 3 demonstrates how melanin blocks light as a result of its high absorption coefficient. Fig. 4 suggests

that when the diffuse reflectance of a short-pulsed laser from a tissue is used for the detection of buried objects, gating off the early-arriving light will enhance the imaging quality in contrast to gating off the late-arriving light when transmitted light is used for imaging. Because the early-arriving reflected light does not propagate deep enough to go through the buried object, it does not contribute useful information to the detection of the buried object.

Our modeling program is merely a tool for simulating practical problems. We hope other interesting problems will be simulated to reveal new features.

ACKNOWLEDGMENTS

We than Linda Eppich for proofreading the manuscript. This research was supported in part by the Office of Naval Research (N00014-91-J-1354), the Air Force Office of Scientific Research (F49620-93-1-0298DEF), and the National Institutes of Health (R29-HL45045).

REFERENCES

1. B. C. Wilson and G. Adam, "A Monte Carlo model for the absorption and flux distributions of light in tissue," Med. Phys. 10, 824-830 (1983).
2. M. Keijzer, S. L. Jacques, S. A. Prahl, and A. J. Welch, "Light distributions in artery tissue: Monte Carlo simulations for finite-diameter laser beams," Lasers Surg. Med. 9, 148-154 (1989).
3. S. L. Jacques and L.-H. Wang, "Monte Carlo modeling of light transport in tissues," in Optical Thermal Response of Laser Irradiated Tissue, edited by A. J. Welch and M. J. C. van Gemert (Plenum Publishing Corp., New York, 1994), in press.
4. S. L. Jacques, "Time resolved propagation of ultrashort laser pulses within turbid tissues," Applied Optics 28 (12), 2223-2229 (1989).
5. S. A. Prahl, M. Keijzer, S. L. Jacques, and A. J. Welch, "A Monte Carlo model of light propagation in tissue," Proc. SPIE 5, 102-111 (1989).
6. R. L. Barbour, H. Graber, J. Lubowsky, and R. Aronson, "Monte Carlo modeling of photon transport in tissue," Biophys. J. 57, 381a-382a (1990).
7. S. T. Flock, B. C. Wilson, D. R. Wyman, and M. S. Patterson, "Monte-Carlo modeling of light-propagation in highly scattering tissues I: model predictions and comparison with diffusion-theory," IEEE Trans. Biomed. Eng. 36 (12), 1162-1168 (1989).
8. T. J. Farrell, M. S. Patterson, and B. C. Wilson, "A diffusion theory model of spatially resolved, steady-state diffuse reflectance for the non-invasive determination of tissue optical properties in vivo," Med. Phys. 19 (4), 879-888 (1992).
9. M. Keijzer, W. M. Star, and P. R. M. Storchi, "Optical diffusion in layered media," Applied Optics 27 (9), 1820-1824 (1988).
10. G. Yoon, S. A. Prahl, and A. J. Welch, "Accuracies of the diffusion approximation and its similarity relations for laser irradiated biological media," Applied Optics 28 (12), 2250-2255 (1989).
11. L.-H. Wang and S. L. Jacques, "Analysis of diffusion theory and similarity relations," Proc. SPIE 1888, 107-116 (1993).
12. K. M. Yoo, F. Liu, and R. R. Alfano, "When does the diffusion approximation fail to describe photon transport in random media?" Phys. Rev. Lett. 64, 2647-2649 (1990).
13. I. Dayan, S. Havlin, G. H. Weiss, "Photon migration in a 2-layer turbid medium - a diffusion analysis," J. Modern Opt. 39 (7), 1567-1582 (1992).
14. A. Ishimaru, "Diffusion of light in turbid material," Applied Optics 28 (12), 2210-2215 (1989).

15. S. J. Madsen, M. S. Patterson, B. C. Wilson, S. M. Jaywant, and A. Othonos, "Numerical modeling and experimental studies of light pulse propagation in inhomogeneous random media," Proc. SPIE 1888, 90-102 (1993).
16. S. R. Arridge, M. Schweiger, M. Hiraoka, and D. T. Delpy, "A finite element approach for modeling photon transport in tissue," Med. Phys. 20, 299-309 (1993).
17. S. T. Flock, B. C. Wilson, and M. S. Patterson, "Hybrid Monte Carlo - diffusion theory modeling of light distributions in tissue," Proc. SPIE 908, 20-28 (1988).
18. L.-H. Wang and S. L. Jacques, "Hybrid model of Monte Carlo simulation diffusion theory for light reflectance by turbid media," J. Opt. Soc. Am. A, 10, 1746-1752 (1993).
19. L.-H. Wang and S. L. Jacques, "Monte Carlo modeling of light transport in multi-layered tissues in standard C," The University of Texas M. D. Anderson Cancer Center, Houston, Texas (1992).
20. Lux and L. Koblinger, Monte Carlo Particle Transport Methods: Neutron and Photon Calculations (CRC Press, 1991).
21 S. L. Jacques, Laser Biology Research Laboratory, The University of Texas M. D. Anderson Cancer Center, Houston, Texas, personal communication, 1993.

FIGURES

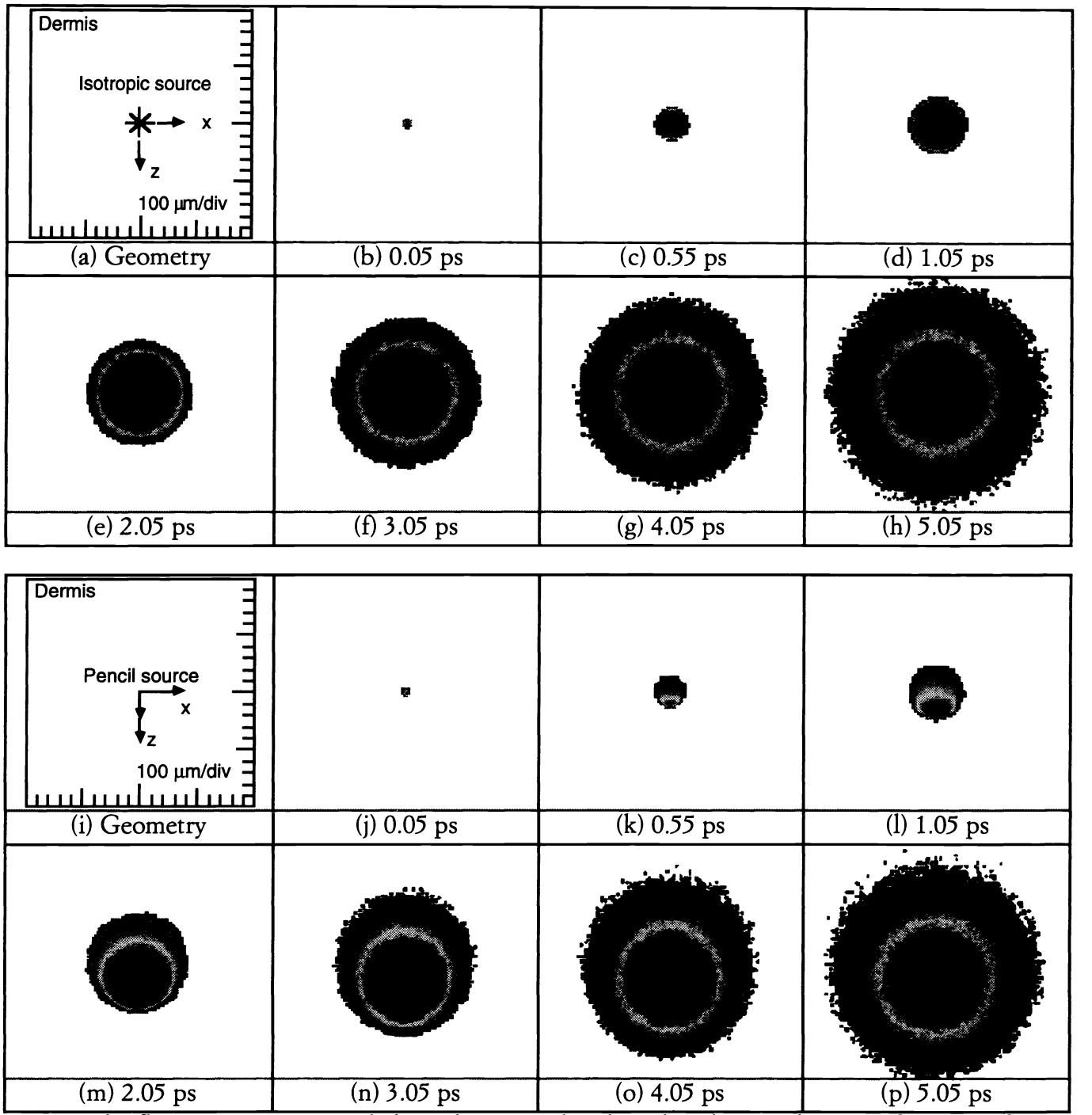

Fig. 1. The fluence rate integrated along the y-axis distributed in the x-z plane as a function of time, where the y-axis points outward from the paper. The top two rows are computational results for an isotropic point source inside a dermis tissue, and the bottom two rows are for a pencil beam. Figs. 1a and 1i are the geometries of the simulations, where the scales are 100 μm/division and the simulation covers a 2 cm × 2 cm area. The light sources are δ-pulses in time. The optical properties of the dermis are: n = 1.37, μ_a = 1.4 cm^{-1}, μ_s = 350 cm^{-1}, and g = 0.8.

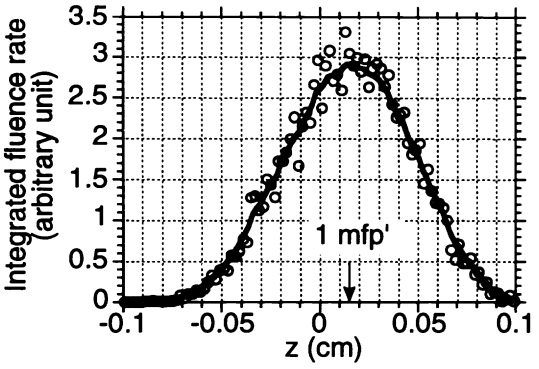

Fig. 2. The fluence rate integrated along the y-axis in Fig. 1p as a function of z.

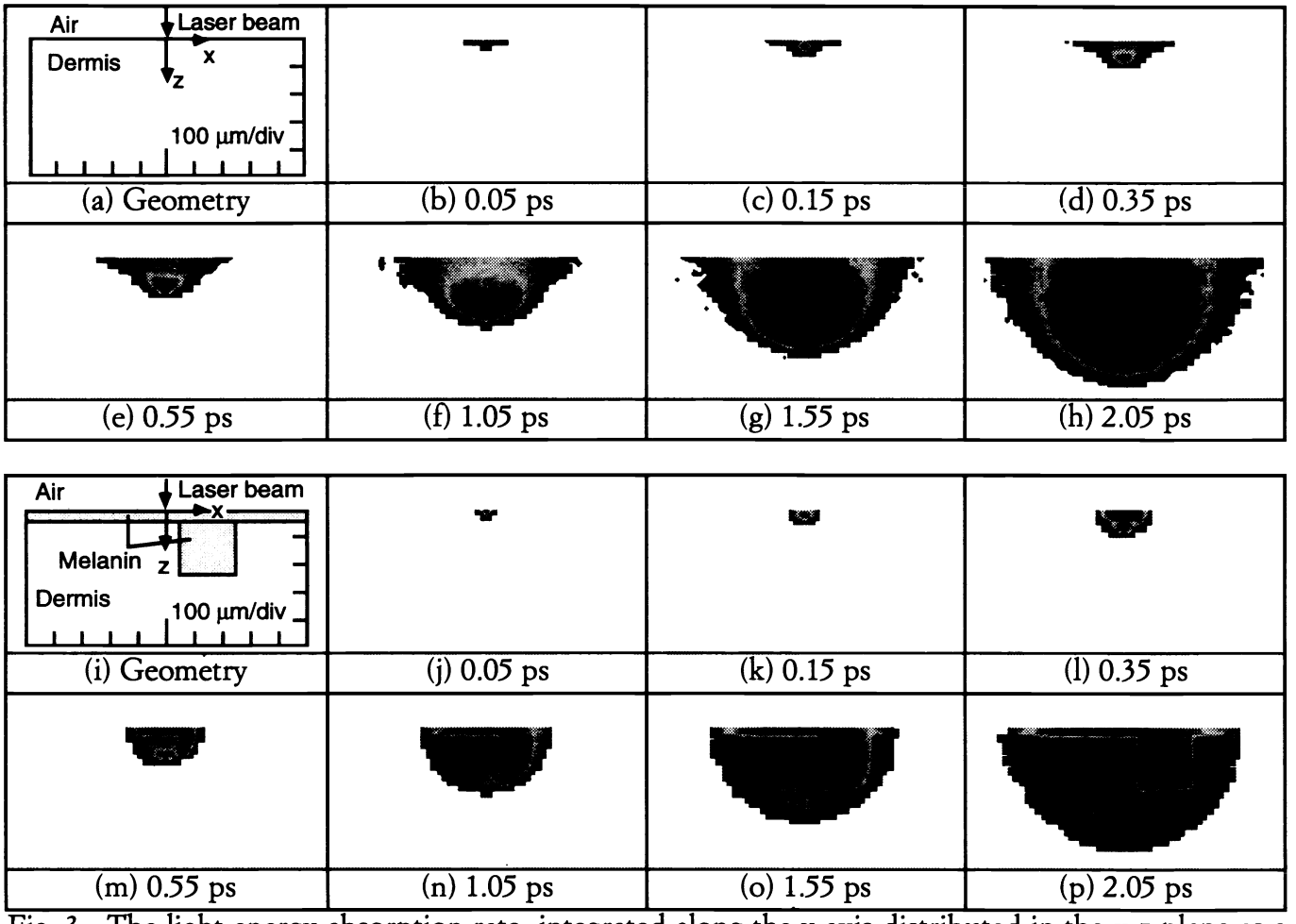

Fig. 3. The light energy-absorption rate integrated along the y-axis distributed in the x-z plane as a function of time, where the y-axis points outward from the paper. The top two rows are computational results for a semi-infinite dermis tissue, and the bottom two rows are for a semi-infinite dermis tissue with buried melanin where the melanin tissue are considered infinitely long along the y-axis. The incident light sources are pencil beams and δ-pulses in time. The optical properties of the dermis at 440 nm wavelength are: n = 1.37, μ_a = 1.4 cm^{-1}, μ_s = 350 cm^{-1}, and g = 0.8. The optical properties of the melanin at 440 nm wavelength are: n = 1.37, μ_a = 48 cm^{-1}, μ_s = 350 cm^{-1}, and g = 0.8.

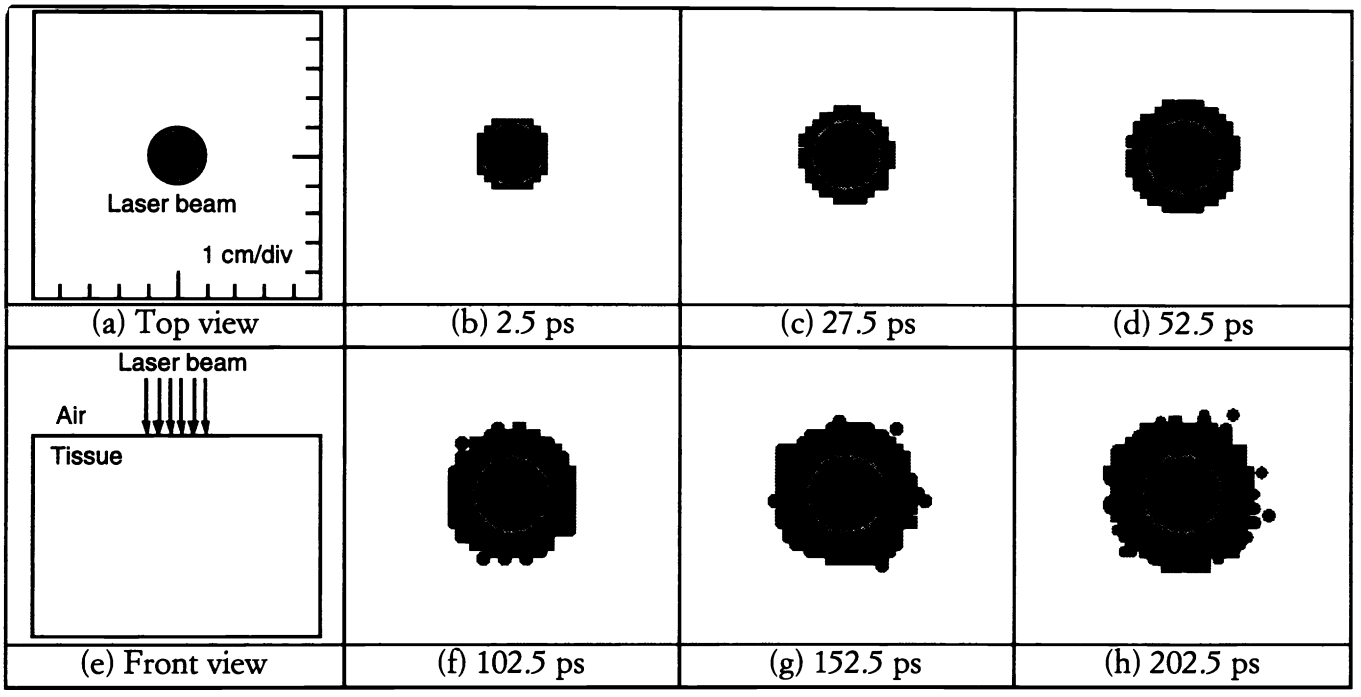

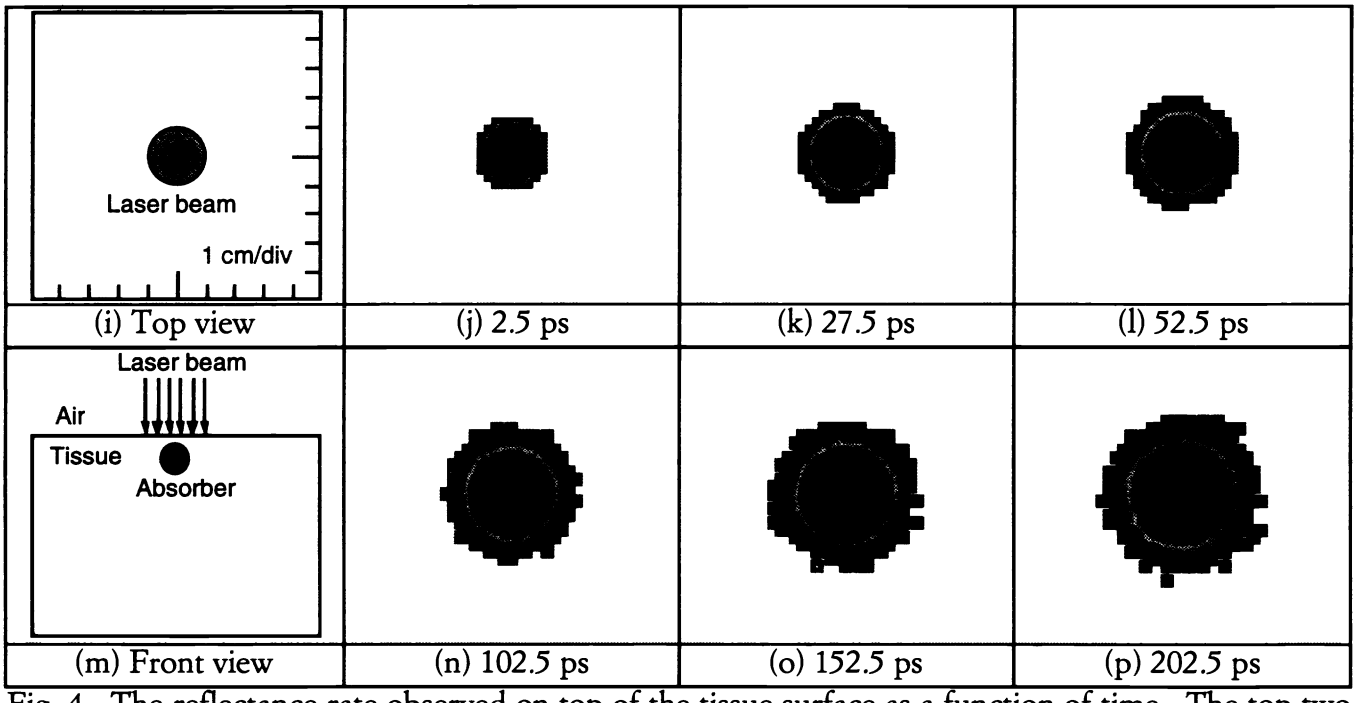

Fig. 4. The reflectance rate observed on top of the tissue surface as a function of time. The top two rows are computational results for a semi-infinite tissue, and the bottom two rows are for a semi-infinite tissue with a buried absorber. The radius of the absorber is 0.5 cm and the center of the absorber is 0.6 cm away from the air-tissue interface. The light sources are δ-pulses in time. The optical properties of the tissue are: n = 1.37, μ_a = 0.1 cm^{-1}, μ_s = 100 cm^{-1}, and g = 0.9. The optical properties of the absorber are: n = 1.37, μ_a = 100 cm^{-1}, μ_s = 100 cm^{-1}, and g = 0.9.